1.D.2:
1.E.3:
1.E.6

Nuclear Physics **A110** (1968) 529—554;

NUCLEAR DEFORMATIONS IN THE PAIRING-PLUS-QUADRUPOLE MODEL (III). Static nuclear shapes in the rare-earth region

KRISHNA KUMAR †
Massachusetts Institute of Technology, Cambridge, Massachusetts
and
Michigan State University, East Lansing, Michigan
and
MICHEL BARANGER
Carnegie Institute of Technology, Pittsburgh, Pennsylvania ††

Received 29 September 1967

Abstract: The potential energy of deformation $\mathscr{V}(\beta, \gamma)$, is calculated with the pairing-plus-quadrupole model for nuclei with $N = 82$-126, $Z = 50$-82. There is a sudden onset of deformation in the $N = 86$-90 region, and the static nuclear shape, the lowest minimum of the potential function, changes from spherical to prolate. The disappearance of deformation in the $Z = 74$-80 region is more gradual, and the static shape changes from prolate to asymmetric to oblate to spherical. The energy of zero-point motion is calculated, and it is concluded that all the stable deformed shapes of the region are prolate. Proton and neutron energy gaps, intrinsic quadrupole moments, moments of inertia and gyromagnetic ratios of the doubly even nuclei of the rare-earth region are calculated and compared with the experimental data.

1. Introduction

Among the most striking low-energy properties of doubly even nuclei are the large variations in the energy and electromagnetic width of the first 2^+ state. For example, as nucleons are added in the $N = 82$–126, $Z = 50$–82 shells (the rare-earth region), the E_{2+} value decreases, and the $B(\mathrm{E2}, 0 \rightarrow 2)$ value increases by a factor††† of 20, then the variation is reversed as one nears the end of the shells. The collective model[2-4]) provides a phenomenological understanding of such variations. The sharp decrease in E_{2+} and the corresponding increase in $B(\mathrm{E2}, 0 \rightarrow 2)$ is associated with a change in the static nuclear shape from spherical to deformed; this onset of deformation causes an increase in the moment of inertia $\mathscr{I} \approx (E_{2+})^{-1}$ and in the intrinsic quadrupole moment $Q_s \approx [B(\mathrm{E2}, 0 \rightarrow 2)]^{\frac{1}{2}}$.

† Present address: Niels Bohr Institute, Copenhagen, Denmark.

†† This work has been supported in part through funds provided by the U.S. Atomic Energy Commission under Contract No. AT(30-1)-2098 at M.I.T., and under Contract No. AT(11-1)(1051 at M.S.U. and by the U.S. Office of Naval Research under Contract No. Nonr 760(15)NR024-439 at C.I.T.

††† A recent compilation is given in ref. [1]).

Now that many nuclear theorists are engaged in trying to justify all nuclear properties from "first principles", it is obviously desirable to understand these collective properties on the basis of the shell model. The explanation cannot be trivial since, in the spherical shell model, the single-particle estimate or Weisskopf [5]) unit for the B(E2) value varies only by a factor 2 throughout the rare-earth region. A valid microscopic theory has to account for the large variations in the excitation energies and the transition probabilities. If such a theory can be found, then it can be used to test some of the assumptions of the collective model, and particularly of its two limiting cases, the vibrational model and the rotational model, which are often used to describe spherical and deformed nuclei, respectively.

Mottelson and Nilsson [6]) determined the static shapes by looking for the lowest minimum of the sum of the energies of the occupied Nilsson levels. They explained the magnitude of the B(E2) values of the deformed nuclei of the rare-earth region, which are about 200 Weisskopf units. However, this kind of calculation predicts deformed shapes for all non-closed shell nuclei and cannot explain the abrupt change of shape. A semi-quantitative explanation was provided by Belyaev [7]) in terms of the competition between a quadrupole force which tries to deform the nucleus and a pairing force which tries to keep it spherical. This calculation was performed for an abstract model in which all the spherical, single-particle levels are degenerate. Bès and Szymański [8]) extended the Mottelson-Nilsson calculation by including the pairing effects. They predict the onset and disappearance of deformation at roughly the correct values of Z and N, but the calculated energy curves are rather shallow and hence the deformed minima are not stable against zero-point motion. Dietrich, Mang and Pradal [9]) have performed a self-consistent calculation using a "realistic" two-body interaction – a Gaussian with suitable exchange mixture. In principle, this theory is capable of explaining the factors of 20, but it is still too difficult to be widely applicable (for further discussion, see ref. [13]), subsect. 7.3).

The possibility of asymmetric or tri-axial shapes has been investigated by Newton [10]) and by Das Gupta and Preston [11]). These calculations are generalizations of those of Mottelson-Nilsson and Bès-Szymański, respectively, and hence are subject to the same criticisms.

In this paper, the third in a series [12-14]), we apply the pairing-plus-quadrupole model to a microscopic calculation of the static nuclear shapes in the rare-earth region. The formalism and some of the notations are given in ref. [12]) (paper I). The justification of the model and the method of calculation of $\mathscr{V}(\beta, \gamma)$ – the potential energy of deformation – are discussed in refs. [13,14]) (papers II and IV), where a more detailed comparison with the work of other authors is also given. Here, we shall simply present the results. Earlier versions of this work have already been reported [15,16]). Some of the usual definitions and the main features of our calculations are summarized in the following.

(i) We use a self-consistent method. The self-consistency condition is satisfied by every solution of the pairing-plus-quadrupole Hamiltonian, i.e. the wave-function

deformation equals the potential deformation. In general, there is more than one solution. The solution corresponding to the lowest minimum of $\mathscr{V}(\beta, \gamma)$ is called the static shape and is denoted by (β_s, γ_s). This shape may be spherical ($\beta_s = 0$), prolate ($\beta_s > 0, \gamma_s = 0$), oblate ($\beta_s < 0, \gamma_s = 0$ or $\beta_s > 0, \gamma_s = 60°$), or asymmetric ($\beta_s \neq 0$, $0° < \gamma_s < 60°$).

(ii) Instead of assuming from the outset that deformed nuclei are axially symmetric and prolate, we study the complete γ-dependence of $\mathscr{V}$. (It is sufficient to vary γ from 0° to 60° for positive values of β, since the function $\mathscr{V}$ is unchanged [2]) under the transformations $\gamma \to -\gamma$ and $\gamma \to \gamma \pm 120°$.) While most of the deformed nuclei are found to be prolate, there is a transition from prolate to asymmetric to oblate† to spherical shapes at the heavy-mass end of the region. The preponderance of axially symmetric shapes (prolate or oblate) can be attributed to the pairing force which favors maximum shape symmetry, axial symmetry over asymmetry and spherical symmetry over axial [15,16]) (further discussion is given in subsect. 2.2). The preponderance of prolate shapes (as compared to oblate ones) has been attributed to the steepness of the walls of the single-particle potential [9,11,17]) whose shape lies in between that of a harmonic oscillator and that of an infinite square well, and to the strong spin-orbit interaction [18]).

(iii) The parameters of the vibrational model (B and C) and those of the rotational model (Q_s and $\mathscr{I}$) are calculated at the lowest minimum of $\mathscr{V}(\beta, \gamma)$. The quantities B, C and $\mathscr{I}$ are calculated by using a self-consistent time-dependent Hartree-Bogolyubov method [14]).

(iv) The stability of the calculated static shapes is tested by calculating the energy of zero-point motion. A deformed static shape is not stable against quantal fluctuations if the energy of zero-point motion is comparable to or larger than the energy gained by deforming the nucleus or if a second minimum of $\mathscr{V}$ occurs in the proximity of the lowest one. In such a case, our static calculation should not be relied upon. A dynamic theory suitable for such transitional nuclei has recently been developed [14,15,16,19]).

(v) While the static approximation has more validity for nuclei that are strongly deformed, the pairing-plus-quadrupole model [which involves among other things a small deformation approximation [13])] does not. Hence, no great accuracy can be expected in the rotational nuclei. For example, the calculated (a) binding energies of deformation and (b) energies of β- and γ-vibrations are probably too large. Better values might be obtainable by including in (a) the effects of zero-point motion in the spherical and deformed states and in (b) the deviations from the harmonic approximation. But this has not been done in view of the crudeness of the present calculation. However, in order to estimate the effects of dynamics on the static properties of a well-deformed nucleus, the full dynamical calculation [19]) (which itself may be somewhat affected by numerical inaccuracies in case of a strongly deformed nucleus) has been performed for $^{172}_{70}$Yb. Results given in table 3 indicate that while the effects of

† The calculated asymmetric and oblate shapes are unstable against zero-point motion.

dynamics on Q_s and $\mathscr{I}$ are small, i.e. the properties of the ground band remain unaffected, the energies of β- and γ-vibrations can be reduced by as much as a factor of 2.

(vi) The choice of the spherical single-particle levels is a very important and tricky problem since it affects the whole calculation. We have tried several different choices including the most popular ones due to Mottelson, Nilsson and Prior [6,20]) and Kisslinger and Sorensen [21]). Our choice (table 1) is close to that of ref. [20]) (which gives fair agreement with the ground-state spins of odd-mass, deformed nuclei of the region) and includes some shifts suggested by a Woods-Saxon potential calculation for the lead region [22]). We have also varied the number of these levels – though the major motivation for this variation is to provide an adequate dynamic theory for the osmium region [19]). In our 1963 calculation [15]), we used a complete oscillator shell plus one level of the upper shell ($i_{\frac{13}{2}}$ for neutrons, $h_{\frac{11}{2}}$ for protons), i.e. 56 neutron levels and 42 proton levels. In our 1965 calculation [16]), we used two complete oscillator shells – the usual one plus the upper shell, i.e. 98 neutron levels and 72 proton levels. In the present calculation, the same number of levels have been used, but the effects of the upper shell have been cut down in the manner discussed in refs. [13,19]). With suitable adjustment of the parameters, the static results are in reasonably good agreement with experiment and are practically independent of the three choices mentioned above. The main difference seems to be that there is no change of sign of Q_s in the osmium isotopes in fig. 4 of ref. [16]), while such a change of sign does appear in fig. 32 of ref. [15]) and in fig. 14 of the present calculation.

(vii) The main purpose of the present calculation is to try to understand and predict the onset and disappearance of nuclear deformation. A secondary purpose is to make a preliminary determination of the parameters of the pairing-plus-quadrupole model. These parameters and probably all the results of this static theory would change somewhat if the effects of quantal fluctuations and the resulting coupling between the vibrational and rotational motions were taken into account. The present paper has been written in the hope that the results presented here may provide some guidance until a more detailed and hence lengthy dynamical calculation becomes available.

2. Discussion of the results

2.1. LIST OF THE EQUATIONS

Details of the theory are given elsewhere [12–14]). The main steps and equations are listed here for the sake of completeness.

(i) The single-particle levels η_i and wave functions $|i\rangle$ are obtained by solving the eigenvalue equation

$$[H_S - \sum_{\mu=0,\,2'} D'_\mu P'_\mu]|i\rangle = \eta_i|i\rangle, \tag{1}$$

where H_S is the spherical shell-model Hamiltonian. The deformation variables D'_μ

have dimensions of energy and are related to the usual β and γ by

$$D'_0 = \hbar\omega\beta\cos\gamma, \qquad D'_{2'} = \hbar\omega\beta\sin\gamma, \tag{2}$$

where $\hbar\omega$ is the oscillator energy (independent of deformation). The quadrupole operators P'_μ are the Hermitian components of the dimensionless single-particle quadrupole operator [13]).

(ii) The Fermi energy $\lambda_\tau(\tau = \text{p, n for protons, neutrons})$ and the pairing potential Δ_τ are determined by solving the BCS equations

$$\sum_i E_i^{-1} = 4G_\tau^{-1}, \tag{3}$$

$$\sum_i v_i^2 = N_\tau, \tag{4}$$

where

$$E_i = [(\eta_i-\lambda_\tau)^2+\Delta_\tau^2]^{\frac{1}{2}}, \tag{5}$$

$$v_i^2 = \tfrac{1}{2}[1-(\eta_i-\lambda_\tau)E_i^{-1}] = 1-u_i^2, \tag{6}$$

G_τ is the pairing force strength and N_τ the total number of protons or neutrons. In the above and the following equations, the sums over single-particle states run over all solutions of eq. (1).

(iii) Steps (i) and (ii) are performed for both protons and neutrons. Then the potential energy of deformation is given by

$$\mathscr{V}(\beta,\gamma) = \tfrac{1}{2}\,\mathrm{Tr}\,(H_\mathrm{S}) + \sum_\tau [\lambda_\tau(N_\tau-\Omega_\tau)-\tfrac{1}{2}\sum_i E_i+\Delta_\tau^2 G_\tau^{-1}]+\tfrac{1}{2}D'^2\chi'^{-1}, \tag{7}$$

where Ω_τ is half the total number of proton or neutron states and χ' the quadrupole force strength in units of energy.

Steps (i)–(iii) are repeated for different (β, γ) sets. The quantity β is varied from 0.0 to 0.7 in steps of 0.05, and γ is varied from 0° to 60° in steps of 10°. The lowest minimum of $\mathscr{V}$ is denoted by $(\beta_\mathrm{s}, \gamma_\mathrm{s})$. Final values of β_s, γ_s are obtained by making a parabolic interpolation around the computed minimum. The following quantities are then calculated at the minimum. The electric quadrupole moment is given by †

$$Q_\mathrm{s} = (\tfrac{16}{5}\pi)^{\frac{1}{2}}\sum_\tau e_\tau \sum_i v_i^2\langle i|Q_0|i\rangle, \tag{8}$$

where e_τ is the effective charge of a proton or a neutron and the usual quadrupole operator $Q_0 = r^2Y_{20}$. The moment of inertia and the gyromagnetic ratio are given by (k denotes the intrinsic axis 1, 2 or 3)

$$\mathscr{I}_k = \mathscr{I}_k^\mathrm{c} + \sum_{ij\tau}(u_iv_j-u_jv_i)^2(E_i+E_j)^{-1}|\langle i|J_k|j\rangle|^2, \tag{9}$$

$$g_k = [g^\mathrm{c}\mathscr{I}_k^\mathrm{c} + \sum_{ij\tau}(u_iv_j-u_jv_i)^2(E_i+E_j)^{-1}|\langle i|m_k|j\rangle\langle j|J_k|i\rangle|]/\mathscr{I}_k, \tag{10}$$

† This relation is valid only when $(\beta_\mathrm{s}, \gamma_\mathrm{s})$ is an axially symmetric shape.

where the moment of inertia of the core is

$$\mathscr{I}_k^c = 4B^cD'^2 \sin^2(\gamma - \tfrac{2}{3}\pi k), \tag{11}$$

the gyromagnetic ratio of the core is †

$$g^c = Z_c^{\frac{2}{3}}[Z_c^{\frac{2}{3}} + N_c^{\frac{2}{3}}]^{-1}, \tag{12}$$

and J_k and m_k are the single-particle angular momentum and magnetic momentum operators. The energies of $\mu = 0$, $2'$ vibrations are given in the harmonic approximation by

$$W_\mu = (C_\mu B_\mu^{-1})^{-\frac{1}{2}}, \tag{13}$$

where

$$C_\mu = \chi'^{-1} - \sum_\tau [\Delta_\tau(c_\mu \dot{\lambda}_\mu + d_\mu \dot{\Delta}_\mu) + \sum_{ij} (u_i v_j + u_j v_i)^2 (E_i + E_j)^{-1} |\langle i|P'_\mu|j\rangle|^2], \tag{14}$$

$$B_\mu = B^c + \tfrac{1}{8} \sum_{i\tau} E_i^{-5} [\Delta_\tau(\langle i|P'_\mu|i\rangle + \dot{\lambda}_\mu) + (\eta_i - \lambda_\tau)\dot{\Delta}_\mu]^2 + \sum_{\tau, j\neq i} (u_i v_j + u_j v_i)^2 (E_i + E_j)^{-3} |\langle i|P'_\mu|j\rangle|^2, \tag{15}$$

$$\dot{\lambda}_\mu = \partial\lambda_\tau/\partial D'_\mu, \qquad \dot{\Delta}_\mu = \partial\Delta_\tau/\partial D'_\mu. \tag{16}$$

The quantities c_μ, d_μ, $\dot{\lambda}_\mu$ and $\dot{\Delta}_\mu$ are computed by using eqs. (30)–(35) (with some obvious changes of notation) of ref. [12]). The energy of zero-point motion, which is a measure of the shape stability, is given by

$$\begin{aligned} \xi_0 &= \tfrac{5}{2} W_0 && \text{if} \quad \beta_s = 0 \\ &= \tfrac{1}{2}(W_0 + W_{2'}) && \text{if} \quad \beta_s \neq 0. \end{aligned} \tag{17}$$

2.2. EXPLANATION OF THE TABLES AND FIGURES

Parameters used in the present calculation are listed in table 1. The s.p. levels have been discussed in sect. 1. Values of G_p and G_n are determined by fitting the proton and neutron odd-even mass differences. Values of χ', $e_n(e_p = 1 + e_n)$ and B_c are chosen so as to get the best overall agreement with the experimental quadrupole moments [or $B(E2; 0 \to 2)$ values] and moments of inertia (or E_{2+}). A detailed discussion is given in ref. [13]).

The calculated results are given in table 2 and will be discussed in the later part of this section. The effects of dynamics [19]) on our results for a well-deformed nucleus are demonstrated in table 3. These effects are appreciable and would be even more significant for nuclei which are soft against γ- and β-vibrations, for example the Os isotopes.

Examples of some potential functions $\mathscr{V}(\beta, \gamma)$ are given in figs. 1–4. The respective static shapes are spherical, prolate, asymmetric and oblate. The energy of zero-

† This estimate for g^c gives better agreement with the experimental data than the estimate $g^c = Z^c/A^c$. It could be tested by measuring the g-value of a closed-shell nucleus for which $g \approx g^c$.

point motion is indicated by dashed curves. The asymmetric minimum of fig. 3 and the oblate minimum of fig. 4 are unstable against zero point motion. The preceding statement applies to all the calculated asymmetric and oblate minima (see table 2) including the case of ^{188}Os which is the most asymmetric nucleus ($\gamma_s = 21.4$ degrees, energy gain over the axially symmetric solution is 0.044 MeV) according to the present calculation †. The nuclear shape changes from prolate to oblate in the $A = 186$–192 region and it is perfectly natural that the static shape becomes asymmetric before becoming oblate. However, the picture of a rigid, asymmetric nucleus [24]) does not seem to be valid, as will be seen shortly.

TABLE 1
Parameters used for the present calculation

	Protons				Neutrons			
	N	l	j	η	N	l	j	η
s.p. levels	4	4	$\frac{9}{2}$	−0.975	5	5	$\frac{11}{2}$	−1.202
		4	$\frac{7}{2}$	−0.30		5	$\frac{9}{2}$	−0.430
		2	$\frac{5}{2}$	−0.265		3	$\frac{7}{2}$	−0.475
		2	$\frac{3}{2}$	−0.015		3	$\frac{5}{2}$	−0.125
		0	$\frac{1}{2}$	0.0		1	$\frac{3}{2}$	−0.150
						1	$\frac{1}{2}$	0.0
	5	5	$\frac{11}{2}$	−0.150				
		5	$\frac{9}{2}$	0.575	6	6	$\frac{13}{2}$	−0.30
		3	$\frac{7}{2}$	0.620		6	$\frac{11}{2}$	0.50
		3	$\frac{5}{2}$	0.970		4	$\frac{9}{2}$	0.445
		1	$\frac{3}{2}$	0.995		4	$\frac{7}{2}$	0.895
		1	$\frac{1}{2}$	1.145		2	$\frac{5}{2}$	0.860
						2	$\frac{3}{2}$	1.110
						0	$\frac{1}{2}$	1.095
G	$27\,A^{-1}$ MeV				$22\,A^{-1}$ MeV			
e	$1+1.5\,ZA^{-1}$				$1.5\,ZA^{-1}$			
χ'	$70\,A^{-1.4}$ MeV							
B^c	$5\times10^{-6}\,A^{\frac{7}{3}}$ MeV^{-3}							

The column η gives spherical, single-particle energies in units of $\hbar\omega = 41.2\,A^{-\frac{1}{3}}$ MeV. The method of choosing the parameters is discussed in the text.

† The static shapes of these nuclei are quite sensitive to dynamic effects, as well as the choice of parameters [19, 23]). A more detailed calculation [19]) indicates that ^{190}Os is the most asymmetric nucleus in this region. Therefore, the potential energy of ^{190}Os rather than that of ^{188}Os, is plotted in fig. 3.

TA

Theoretical values of the st

Z	N	A	β_s	γ_s	λ_p	Δ_p	λ_n	Δ_n	
1	2	3	4	5	6	7	8	9	
$_{56}$Ba	82	138	0.0	0.0	−2.971	1.558	−8.779	0.0	2.
	84	140	0.0	0.0	−2.943	1.528	−4.978	0.913	2.
$_{58}$Ce	82	140	0.0	0.0	−2.659	1.686	−8.751	0.0	2.
	84	142	0.0	0.0	−2.636	1.654	−4.932	0.895	2.
	86	144	0.0	0.0	−2.613	1.624	−4.650	1.198	2.
$_{60}$Nd	82	142	0.0	0.0	−2.357	1.766	−8.723	0.0	2.
	84	144	0.0	0.0	−2.338	1.734	−4.887	0.878	2.
	86	146	0.0	0.0	−2.319	1.703	−4.610	1.176	3.
	88	148	0.184	0.0	−2.546	1.393	−5.220	0.972	4.
	90	150	0.242	0.0	−2.699	1.213	−5.232	0.974	5.
$_{62}$Sm	84	146	0.0	0.0	−2.047	1.778	−4.844	0.861	2.
	86	148	0.0	0.0	−2.032	1.746	−4.572	1.155	3.
	88	150	0.196	0.0	−2.214	1.397	−5.285	0.913	4.
	90	152	0.255	0.0	−2.327	1.204	−5.288	0.937	5.
	92	154	0.312	0.0	−2.436	1.006	−5.206	0.901	6.
$_{64}$Gd	84	148	0.0	0.0	−1.761	1.793	−4.801	0.845	2.
	86	150	0.0	0.0	−1.751	1.761	−4.534	1.134	4.
	88	152	0.20	0.0	−1.856	1.393	−5.278	0.878	4.
	90	154	0.255	0.0	−1.917	1.202	−5.255	0.912	5.
	92	156	0.304	0.0	−1.964	1.042	−5.147	0.895	6.
	94	158	0.322	0.0	−1.968	0.976	−4.831	0.877	7.
	96	160	0.330	0.0	−1.963	0.935	−4.477	0.838	7.
$_{66}$Dy	90	156	0.249	0.0	−1.492	1.200	−5.172	0.893	6.
	92	158	0.289	0.0	−1.498	1.058	−5.046	0.896	6.
	94	160	0.310	0.0	−1.497	0.983	−4.765	0.871	7.
	96	162	0.320	0.0	−1.493	0.939	−4.422	0.827	7.
	98	164	0.328	0.0	−1.489	0.903	−4.013	0.748	7.
$_{68}$Er	94	162	0.298	0.0	−1.013	0.981	−4.685	0.864	7.
	96	164	0.311	0.0	−1.002	0.925	−4.362	0.816	7.
	98	166	0.319	0.0	−0.996	0.884	−3.962	0.736	7.
	100	168	0.326	0.0	−0.991	0.849	−3.493	0.680	7.
	102	170	0.331	0.0	−0.987	0.819	−2.931	0.623	7.
$_{70}$Yb	94	164	0.279	0.0	−0.544	1.013	−4.559	0.871	6.
	96	166	0.297	0.0	−0.499	0.943	−4.274	0.815	7.
	98	168	0.308	0.0	−0.474	0.894	−3.894	0.735	7.
	100	170	0.316	0.0	−0.457	0.854	−3.437	0.681	7.
	102	172	0.320	0.0	−0.446	0.820	−2.900	0.632	7.
	104	174	0.314	0.0	−0.456	0.810	−2.376	0.738	7.
	106	176	0.310	0.0	−0.463	0.798	−1.961	0.805	7.
$_{72}$Hf	94	166	0.252	0.0	−0.188	1.061	−4.363	0.909	6.
	96	168	0.274	0.0	−0.103	1.004	−4.128	0.841	6.
	98	170	0.290	0.0	−0.045	0.962	−3.791	0.758	7.
	100	172	0.299	0.0	−0.014	0.932	−3.360	0.706	7.

2
deformation and related quantities

E_S	ξ_0	$\mathscr{I}$	g	B_0	C_0	W_0	$B_{2'}$	$C_{2'}$	$W_{2'}$
11	12	13	14	15	16	17	18	19	20
0.0	6.918	1.084	0.437	0.826	6.323	2.767	0.826	6.323	2.767
0.0	5.015	1.496	0.367	1.023	4.115	2.006	1.023	4.115	2.006
0.0	6.327	1.185	0.462	0.890	5.702	2.531	0.890	5.702	2.531
0.0	4.431	1.693	0.389	1.100	3.454	1.772	1.100	3.454	1.772
0.0	2.737	2.741	0.347	1.280	1.534	1.095	1.280	1.534	1.095
0.0	5.879	1.276	0.480	0.947	5.238	2.352	0.947	5.238	2.352
0.0	3.980	1.884	0.404	1.168	2.960	1.592	1.168	2.960	1.592
0.0	2.155	3.480	0.361	1.358	1.009	0.862	1.358	1.009	0.862
0.867	1.687	12.166	0.284	1.511	3.818	1.590	1.443	4.592	1.784
2.703	1.706	20.699	0.299	1.759	4.152	1.536	1.495	5.262	1.876
0.0	3.637	2.062	0.415	1.232	2.606	1.455	1.232	2.606	1.455
0.0	1.664	4.507	0.370	1.430	0.634	0.666	1.430	0.634	0.666
1.201	1.709	14.320	0.293	1.536	4.215	1.657	1.514	4.698	1.761
3.111	1.557	23.339	0.304	2.164	3.411	1.255	1.564	5.399	1.858
5.321	1.404	35.821	0.288	3.426	1.762	0.717	1.509	6.602	2.092
0.0	3.389	2.213	0.423	1.294	2.379	1.356	1.294	2.379	1.356
0.0	1.255	5.978	0.378	1.502	0.378	0.502	1.502	0.378	0.502
1.339	1.698	15.354	0.299	1.581	4.415	1.671	1.583	4.713	1.725
3.297	1.557	23.968	0.306	2.139	3.916	1.353	1.682	5.216	1.761
5.518	1.355	34.271	0.283	3.248	2.477	0.873	1.733	5.853	1.838
7.680	1.483	37.742	0.289	2.798	4.432	1.259	1.934	5.634	1.707
9.607	1.567	40.373	0.286	2.304	6.462	1.675	2.367	5.041	1.459
3.229	1.640	23.490	0.309	1.917	4.873	1.594	1.780	5.061	1.686
5.335	1.419	31.624	0.288	2.647	3.956	1.223	1.976	5.157	1.615
7.418	1.529	36.145	0.282	2.348	5.605	1.545	2.185	5.000	1.513
9.301	1.652	39.102	0.276	1.896	7.671	2.011	2.647	4.427	1.293
10.883	1.946	43.409	0.254	1.378	9.879	2.677	2.998	4.419	1.214
6.808	1.672	34.686	0.279	2.025	6.467	1.787	2.162	5.236	1.556
8.666	1.780	38.352	0.271	1.717	8.299	2.199	2.603	4.825	1.362
10.208	2.006	43.075	0.248	1.372	10.195	2.726	2.957	4.886	1.285
11.299	2.357	45.282	0.256	1.262	11.285	2.990	2.289	6.800	1.723
11.821	2.264	48.059	0.252	1.818	10.946	2.454	1.913	8.226	2.074
5.848	1.770	31.761	0.272	1.911	6.850	1.893	2.055	5.565	1.646
7.556	1.865	36.619	0.263	1.730	8.250	2.184	2.365	5.653	1.546
9.023	1.990	41.932	0.242	1.585	9.671	2.470	2.639	6.007	1.509
10.062	2.318	44.504	0.251	1.557	10.518	2.599	1.940	8.040	2.036
10.592	2.315	47.024	0.252	2.227	10.179	2.138	1.531	9.510	2.492
10.325	2.163	43.479	0.280	1.999	9.442	2.173	1.795	8.318	2.153
9.701	1.714	40.661	0.309	2.734	7.483	1.654	2.188	6.879	1.773
4.562	1.717	26.320	0.252	1.814	7.128	1.982	2.205	4.645	1.451
6.102	1.820	31.924	0.229	1.699	8.071	2.180	2.389	5.096	1.461
7.421	1.876	37.635	0.205	1.741	8.835	2.253	2.557	5.749	1.500
8.366	2.108	40.434	0.209	1.848	9.217	2.233	1.947	7.655	1.983

TABLE

Z	N	A	β_s	γ_s	λ_p	Δ_p	λ_n	Δ_n	Q
1	2	3	4	5	6	7	8	9	1
$_{72}$Hf	102	174	0.302	0.0	−0.003	0.907	−2.866	0.677	7.4
	104	176	0.295	0.0	−0.030	0.892	−2.380	0.741	7.3
	106	178	0.285	0.0	−0.071	0.881	−1.957	0.783	7.1
	108	180	0.273	0.0	−0.124	0.876	−1.521	0.824	6.9
	110	182	0.261	0.0	−0.176	0.875	−1.140	0.917	6.6
$_{74}$W	98	172	0.264	0.0	0.273	0.962	−3.650	0.819	6.4
	100	174	0.275	0.0	0.318	0.940	−3.265	0.767	6.7
	102	176	0.277	0.0	0.323	0.918	−2.832	0.751	6.8
	104	178	0.269	0.0	0.280	0.893	−2.400	0.780	6.6
	106	180	0.259	0.0	0.229	0.872	−1.984	0.796	6.4
	108	182	0.248	0.0	0.166	0.856	−1.560	0.836	6.2
	110	184	0.228	0.0	0.070	0.854	−1.240	0.932	5.8
	112	186	0.201	0.0	−0.052	0.873	−1.047	0.988	5.2
$_{76}$Os	106	182	0.235	0.0	0.601	0.785	−2.013	0.838	5.7
	108	184	0.221	0.0	0.516	0.763	−1.632	0.887	5.4
	110	186	0.199	0.0	0.392	0.760	−1.362	0.970	5.0
	112	188	0.180	21.4	0.199	0.790	−1.252	0.993	4.4
	114	190	−0.170	10.5	0.054	0.834	−1.160	0.994	−4.5
	116	192	−0.152	0.0	−0.009	0.851	−0.947	0.935	−4.1
$_{78}$Pt	106	184	0.203	0.0	0.934	0.752	−2.054	0.939	4.8
	108	186	0.188	0.0	0.831	0.722	−1.735	0.984	4.4
	110	188	0.170	20.2	0.601	0.672	−1.564	1.050	4.0
	112	190	−0.155	0.0	0.331	0.682	−1.447	1.092	−4.1
	114	192	−0.144	0.0	0.288	0.681	−1.215	1.038	−3.9
	116	194	−0.134	0.0	0.250	0.681	−0.978	0.951	−3.6
	118	196	−0.125	0.0	0.218	0.680	−0.714	0.817	−3.4
	120	198	−0.099	0.0	0.159	0.704	−0.436	0.726	−2.8
	112	192	−0.135	0.0	0.679	0.001	−1.465	1.113	−3.5
$_{80}$Hg	114	194	−0.128	0.0	0.653	0.001	−1.235	1.050	−3.4
	116	196	−0.116	0.0	0.658	0.0	−1.005	0.969	−3.1
	118	198	−0.099	0.0	0.662	0.270	−0.760	0.872	−2.8
	120	200	−0.080	0.0	0.547	0.415	−0.504	0.774	−2.2
	122	202	0.0	0.0	0.322	0.606	−0.362	0.749	−3.5
	124	204	0.0	0.0	0.313	0.596	−0.065	0.510	−2.7
$_{82}$Pb	118	200	0.0	0.0	0.611	0.001	−0.838	1.011	−3.6
	120	202	0.0	0.0	0.599	0.001	−0.609	0.894	−3.3
	122	204	0.0	0.0	0.586	0.001	−0.369	0.734	−2.9
	124	206	0.0	0.0	0.574	0.001	−0.073	0.497	−2.5
	126	208	0.0	0.0	0.563	0.001	0.302	0.0	−3.0

The method of calculation is described in sect. 2. A deformed shape is unstable and hence unreliable if the ze point energy (column 12) is equal to or larger than the binding energy of deformation (column 11). Values gi in columns 10, 13 and 14 for the spherical and asymmetric shapes have been obtained by using the methods scribed in subsect. 2.2. The quantities in the columns are as follows: column 4-static deformation, column asymmetry variable in degrees, column 6 - proton Fermi energy in MeV, column 7 - proton pairing potential MeV, column 8 - neutron Fermi energy in MeV, column 9 - neutron pairing potential in MeV, column 1 intrinsic quadrupole moment in $e \cdot$ b. (A negative sign is used whenever the potential energy function is lo

(continued)

E_s	ξ_0	$\mathscr{I}$	g	B_0	C_0	W_0	$B_{2'}$	$C_{2'}$	$W_{2'}$
11	12	13	14	15	16	17	18	19	20
8.785	2.125	41.854	0.215	2.505	8.858	1.880	1.585	8.902	2.370
8.661	2.159	39.104	0.231	1.857	9.587	2.272	1.863	7.794	2.046
8.135	1.977	35.690	0.253	1.794	9.656	2.320	2.323	6.197	1.633
7.181	1.683	33.250	0.267	2.022	8.664	2.070	2.759	4.635	1.296
5.819	1.309	30.052	0.292	2.556	6.338	1.575	3.064	3.329	1.042
5.671	1.692	31.960	0.194	1.917	8.167	2.064	2.634	4.586	1.319
6.496	1.814	35.147	0.191	2.156	8.226	1.953	2.202	6.176	1.675
6.881	1.856	35.854	0.199	2.548	8.197	1.793	1.934	7.115	1.918
6.855	1.943	35.984	0.207	1.964	9.506	2.200	2.195	6.240	1.686
6.460	1.931	31.571	0.222	1.657	10.380	2.503	2.639	4.879	1.360
5.651	1.712	29.084	0.241	1.794	9.996	2.360	3.045	3.447	1.064
4.510	1.436	24.449	0.277	2.028	8.943	2.100	3.327	1.986	0.773
3.377	1.211	19.084	0.311	2.163	8.461	1.978	3.504	0.688	0.443
4.705	1.683	27.865	0.219	1.866	9.971	2.311	3.083	3.431	1.055
4.068	1.485	24.888	0.243	2.050	9.744	2.180	3.421	2.128	0.789
3.222	1.233	20.116	0.280	2.199	9.078	2.032	3.667	0.690	0.434
2.404	1.248	13.304	0.293	2.517	7.853	1.766	3.247	1.727	0.729
1.942	1.164	15.082	0.278	2.218	7.605	1.852	4.365	0.994	0.477
1.583	1.234	11.741	0.280	2.218	7.609	1.852	4.431	1.680	0.616
2.769	1.226	20.728	0.164	2.353	8.026	1.847	3.824	1.398	0.605
2.353	1.018	17.847	0.183	2.415	8.037	1.827	4.185	0.187	0.211
1.873	1.259	11.851	0.223	2.561	7.097	1.664	3.127	2.281	0.854
1.566	1.069	11.652	0.269	2.203	7.325	1.823	4.188	0.413	0.314
1.342	1.173	10.596	0.282	2.218	7.429	1.830	4.367	1.164	0.516
1.097	1.322	9.937	0.285	2.328	7.457	1.790	4.217	3.071	0.853
0.846	1.471	9.927	0.271	2.759	7.304	1.627	3.670	6.346	1.315
0.469	1.296	7.307	0.282	4.325	5.028	1.078	3.549	8.132	1.514
0.930	1.416	11.359	0.426	2.183	8.099	1.926	3.524	2.892	0.906
0.773	1.495	10.964	0.448	2.206	8.434	1.955	3.674	3.935	1.035
0.608	1.560	10.367	0.485	2.408	8.219	1.848	3.538	5.732	1.273
0.385	0.998	8.532	0.465	15.848	3.136	0.445	3.248	7.819	1.552
0.147	1.091	5.906	0.421	9.357	2.483	0.515	3.351	9.302	1.666
0.0	1.425	5.264	0.255	6.190	2.011	0.570	6.190	2.011	0.570
0.0	2.525	2.971	0.264	6.239	6.362	1.010	6.239	6.362	1.010
0.0	2.172	3.453	0.076	4.022	3.036	0.869	4.022	3.036	0.869
0.0	2.404	3.119	0.068	4.578	4.234	0.962	4.578	4.234	0.962
0.0	2.823	2.657	0.062	5.105	6.508	1.129	5.105	6.508	1.129
0.0	3.650	2.055	0.063	5.125	10.926	1.460	5.125	10.926	1.460
0.0	9.379	0.800	0.226	1.454	20.464	3.752	1.454	20.464	3.752

on the oblate side than on the prolate side), column 11 binding energy of deformation $\mathscr{V}(0,0)-\mathscr{V}(\beta_s,\gamma_s)$, in MeV, column 12 - zero-point energy in MeV, which is the approximate position of the nuclear ground state above the lowest minimum of $\mathscr{V}$, column 13 - moment of inertia in MeV^{-1}, column 14 - gyromagnetic ratio, which includes the spin contribution, column 15 - vibrational kinetic coefficient [for $\mu = 0$ vibrations in D_0', defined by eq. (2)] in MeV^{-3}, column 16 - stiffness coefficient in MeV^{-1}, column 17 - energy of a $\mu = 0$ phonon, which corresponds to a β-vibration if $\beta_s \neq 0$, $\gamma_s = 0$ and columns 18-20—quantities for $\mu = 2'$ vibrations, which correspond to γ-vibrations if $\beta_s \neq 0, \gamma_s = 0$.

TABLE 3

Effects of dynamics on the static properties of the well-deformed nucleus ^{172}Yb

	S.M.	D.M.	% Diff.	Expt.
Q_s	7.9	8.2	4.0	7.8 [a])
$\mathcal{I}$	47.0	47.0	0.0	38.1 [a])
g	0.25	0.27	8.0	0.304 [b])
E_4/E_2	3.3	3.3	0.0	3.3 [c])
W_β	2.1	1.3	−38.0	1.045 [d])
W_γ	2.5	2.0	−20.0	1.468 [c])
ξ_0	2.3	3.3	43.0	

[a]) Ref. [1]). [b]) Ref. [28]). [c]) Ref. [26]). [d]) Ref. [38]).

The S.M. (static method) quantities have been taken from table 2. The D.M. (dynamic method) quantities have been calculated by using the method of ref. [19]). The same parameters are used for the two calculations.

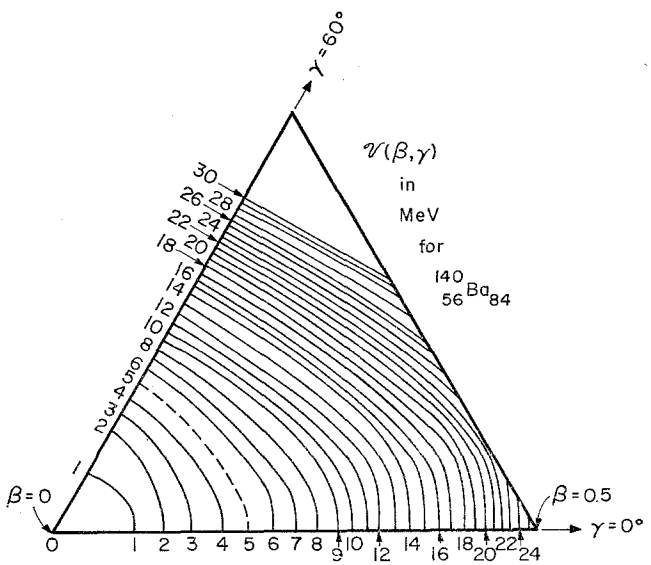

Fig. 1. The potential energy function $\mathcal{V}(\beta, \gamma)$ for ^{140}Ba. The solid lines are contours of constant $\mathcal{V}$. The dashed curve in figs. 1-4 represents the zero-point energy calculated in the harmonic approximation. (Deviations from the harmonic approximation and from the A-dependence of the parameters (table 1) would reduce this energy, which is undoubtedly too large, especially for cases with $\beta_s = 0$.) The lowest minimum occurs for a spherical shape ($\beta_s = 0$). This potential function and those that follow are not reliable at large deformations such as those occurring in nuclear fission [34]) for reasons explained in ref. [13]).

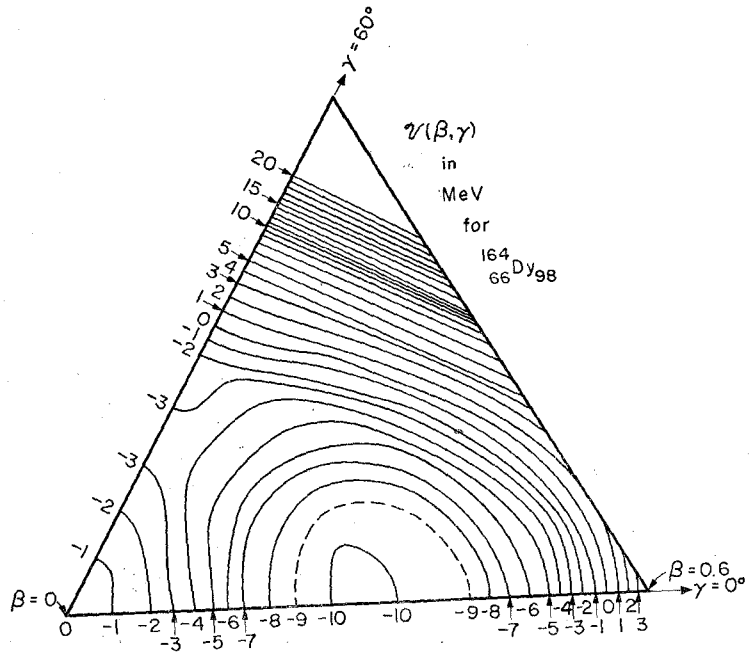

Fig. 2. Contour map of $\mathscr{V}(\beta,\gamma)$ for ^{164}Dy. The only true minimum occurs for a deformed, prolate shape with $\beta_s = 0.328$, $\gamma_s = 0$. There is a second stationary point (a saddle shape since it is a minimum in the β-direction but a maximum in the γ-direction) at $\beta = 0.269$, $\gamma = 60°$ which corresponds to an oblate shape and lies 7.2 MeV above the prolate minimum. The potential function always has a stationary point at $\beta = 0$. It is a maximum in the present case and lies 10.9 MeV above the prolate minimum. Hence the binding energy of deformation is about 11 MeV. This value and similar ones for neighboring nuclei appear to be larger than is required by experiment [34,35]). Discussion is given in

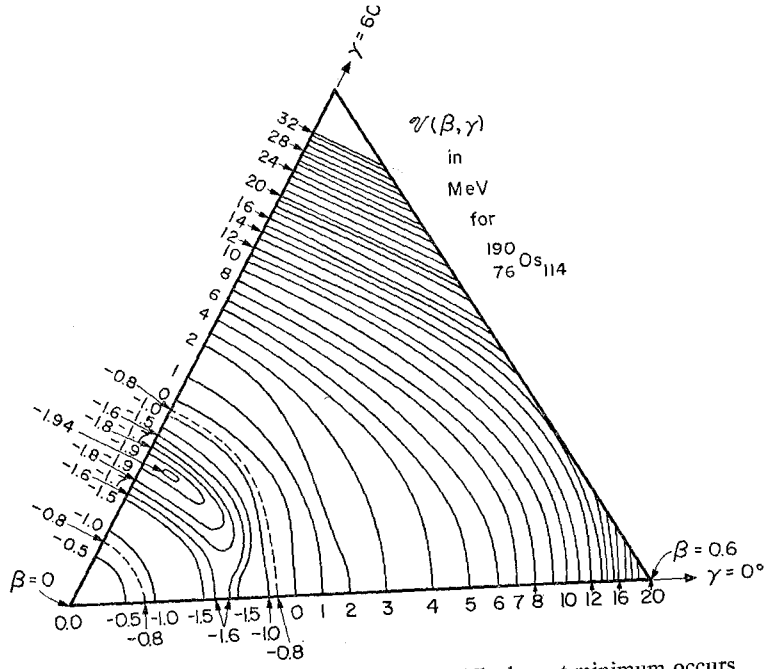

Fig. 3. Contour map of $\mathscr{V}(\beta,\gamma)$ for ^{190}Os. The lowest minimum occurs for a deformed, asymmetric (ref. [23])) shape with $\beta_s = 0.17$, $\gamma_s = 50°$ or $\beta_s = -0.17$, $\gamma_s = 10°$. This minimum is very shallow and is only 0.008 MeV below the saddle shape at $\beta = -0.17$, $\gamma = 0°$. Hence it should be easily washed out by quantal fluctuations [19]). Obviously, deviations from the harmonic approximation are large and the calculated zero point energy is unreliable. This also applies to fig. 4. The nucleus is soft towards γ-vibrations and the corresponding energy is quite low. Further discussion is given in subsect. 2.2.

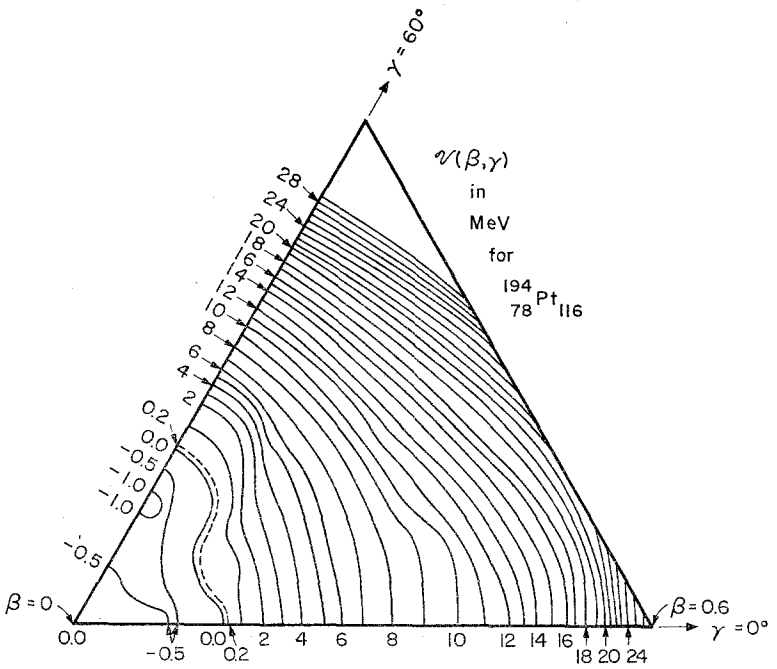

Fig. 4. Contour map of $\mathscr{V}(\beta,\gamma)$ for ^{194}Pt. The lowest minimum occurs for a deformed, oblate shape with $\beta_s = 0.134$, $\gamma_s = 60°$ or $\beta_s = -0.134$, $\gamma_s = 0$. Additional stationary points of $\mathscr{V}$ are a saddle point, prolate shape at $\beta = 0.097$ and a maximum at $\beta = 0$. The corresponding energies are 0.565 and 1.097 MeV above the oblate minimum. The oblate shape is unstable since the zero point energy curve lies 0.2 MeV above the spherical hump at $\beta = 0$.

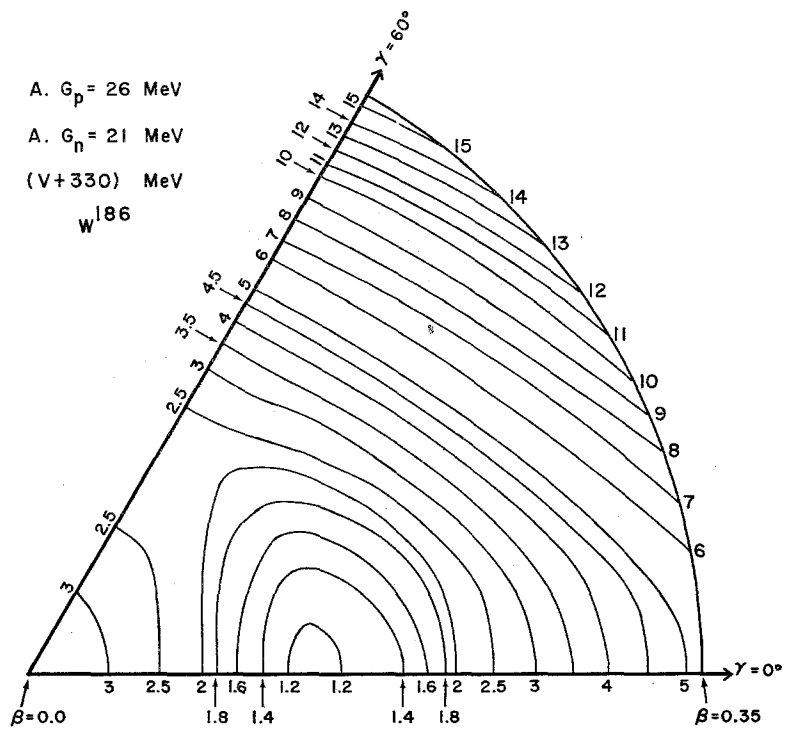

Fig. 5. Plot of $\mathscr{V}(\beta,\gamma)$ of $^{186}_{74}W_{112}$ calculated with the normal strengths of proton and neutron pairing forces. The static shape is deformed, axially symmetric.

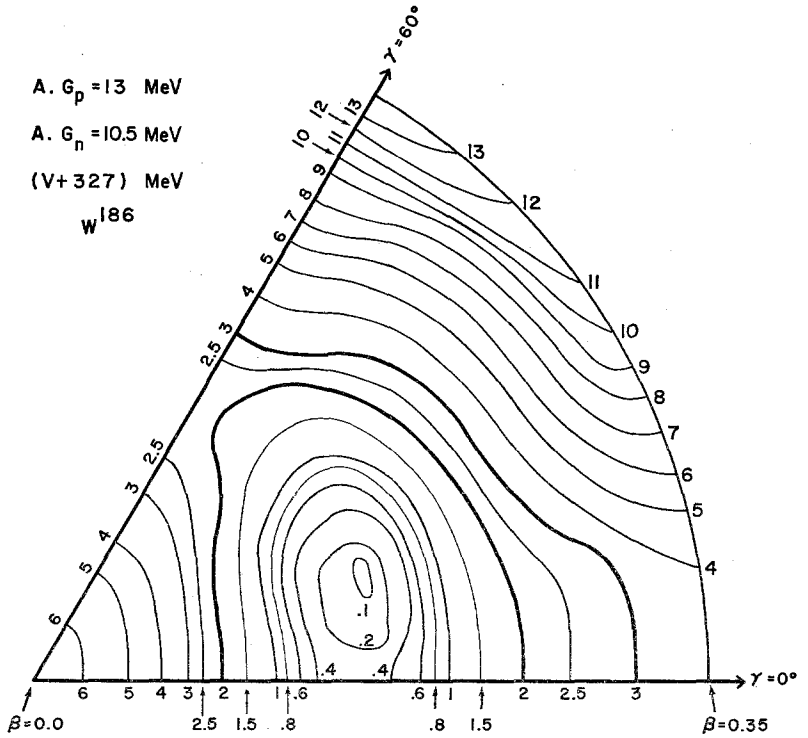

Fig. 6. Plot of $\nu(\beta,\gamma)$ of ^{186}W calculated with weaker pairing forces (50 %) than fig. 5. The static shape is deformed, asymmetric. However, the energy gain over the prolate shape is only 0.3 MeV.

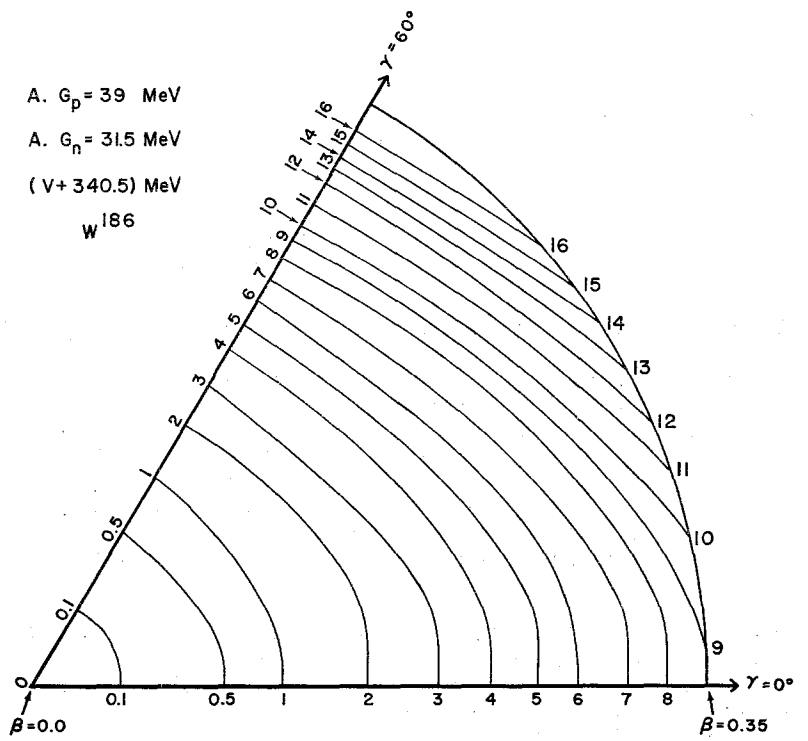

Fig. 7. Plot of $\nu(\beta,\gamma)$ of ^{186}W calculated with stronger (150 %) pairing forces than fig. 5. The static shape is spherical.

The effect of the pairing force on the shape symmetry is demonstrated in figs. 5–7. Fig. 5 gives $\mathscr{V}(\beta, \gamma)$ for ^{186}W calculated with normal † strengths of proton and neutron pairing forces. The static nuclear shape is deformed, axially symmetric ($\gamma_s = 0°$). When the pairing strengths are reduced by 50 % (fig. 6), the lowest minimum of $\mathscr{V}$ corresponds to an asymmetric shape. However, the energy gain over the axial shape is only 0.3 MeV. When the pairing force strengths are increased by 50 % (fig. 7), the nuclear shape becomes spherical. These results show that in

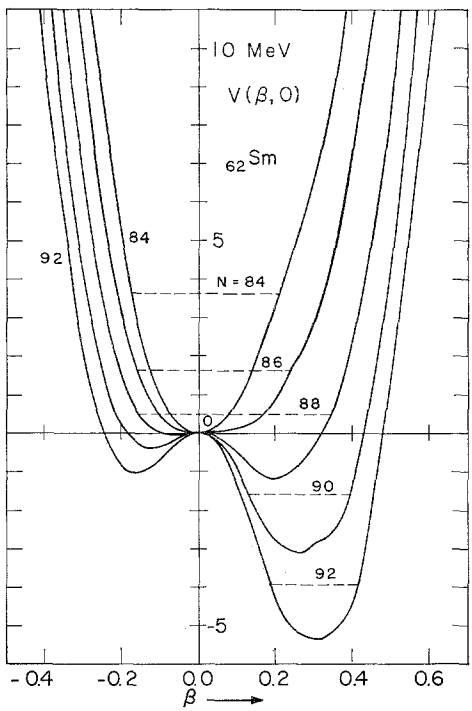

Fig. 8. The onset of nuclear deformation in the samarium isotopes. This is a plot of $\mathscr{V}$ versus β for $\gamma = 0$. The energy of zero-point motion or the approximate location of the ground state is indicated by dotted lines. The deformation sets in suddenly as the neutron number reaches 90. For $N = 88$, there is a deformed minimum, but the zero-point energy is larger than the energy gain due to deformation, showing that the nucleus is transitional rather than deformed. This calculation of the zero-point energy in a transitional nucleus, being based on the harmonic approximation, is quantitatively unreliable. A reliable calculation would follow the lines of ref. [19]) but would not alter the fact that this nucleus is not permanently deformed. For $N = 90$, the minimum is already several MeV deep and the ground state is well below the spherical hump, so that this nucleus should be well-deformed. One can also see how prolate deformations ($\beta > 0$) are much preferred over oblate ($\beta < 0$).

† Potential functions given in figs. 5-7 have been calculated [16]) with parameters which are somewhat different from those used for the rest of this paper. However, we have tested [15,16]) the symmetrizing effects of the pairing force for many combinations of parameters (and for many regions of the nuclear chart) and believe that the effects are independent of the parameters of the model, as well as the number of nucleons in the nucleus.

general the pairing force likes to keep the nucleus as symmetric as possible. A strong pairing force produces complete symmetry (spherical shape); a weaker one gives axial symmetry; a weaker one yet, or no pairing force, yields complete asymmetry.

There follows that the existence of nuclei with rigid asymmetric shape must be quite unlikely. With reasonable strength of the pairing force, very few asymmetric minima are found and they are always very shallow. Even with an unreasonably weak

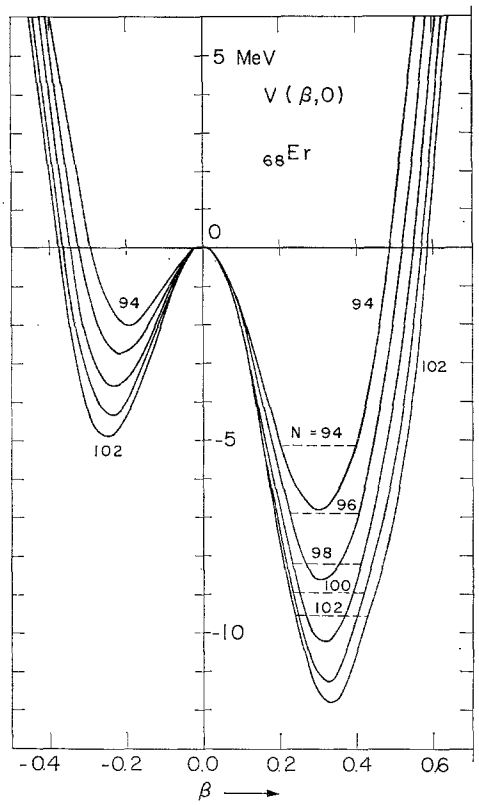

Fig. 9. Nuclear deformation in the erbium isotopes. In contrast to fig. 8, there is no sudden change as the neutron number is increased from 94 to 102, but the binding energy of deformation increases from 7 to 12 MeV, and the prolate-oblate difference increases from 5 to 7 MeV.

pairing force, as has just been seen, the asymmetric minima that are found are still shallow (a few tenths of MeV). Such weak minima are not capable of supporting a stable rigid shape and will be washed out by zero-point motion.

The reason for this symmetrizing effect of the pairing force must be sought in the fact that, by blurring out the Fermi surface, pairing effects decrease the importance of any special ordering of single-particle levels. In consequence, the potential energy of deformation $\mathscr{V}(\beta, \gamma)$ is smoothed out gradually as the pairing strength increases. First to be smoothed out are the features involving the least amount of energy, such

as the asymmetric minima or maxima. For stronger pairing, the oblate-prolate difference and the deformed minimum itself, which involve a few MeV, would also become smoothed out.

The effects of nucleon number on the static shape, prolate-oblate difference and shape stability are demonstrated in figs. 8–10 which give $\mathscr{V}$ versus β for three series of isotopes. Figs. 11–12 give some of the calculated single-proton and single-neutron levels versus β. Values of the odd-even mass differences, intrinsic quadrupole

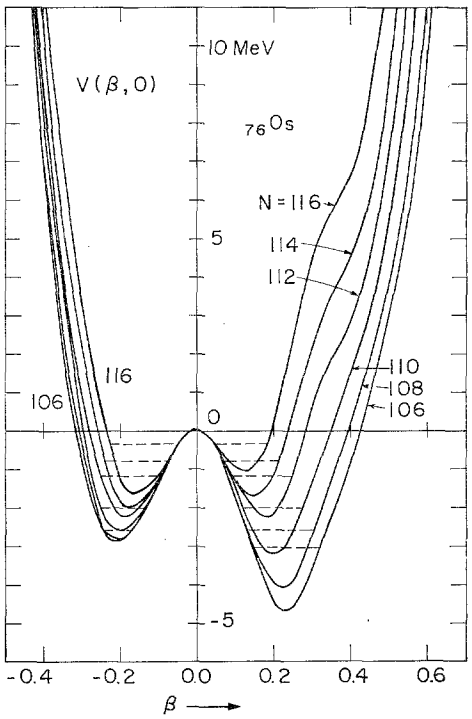

Fig. 10. The transition from prolate to oblate shapes in the osmium isotopes. In contrast to fig. 8, the deformation disappears rather slowly at the heavy-mass end of the region. In fact, it has not quite disappeared in the Os isotopes. The magnitude of the deformation β decreases as N is increased from 106 to 116. (The deformation decreases more rapidly if Z is increased instead of N, which is reasonable in view of the proximity of the magic number $Z = 82$.) At the same time, there is a change in γ so that the static shape goes from prolate at $N = 106$-110 through asymmetric at $N = 112$-114 (the complete plot for ^{190}Os is given in fig. 3) to oblate at $N = 116$. Since the energy difference between prolate, oblate and spherical solutions (especially the first two) is rather small, details of this picture can be expected to be washed out by the quantal fluctuations.

moments, moments of inertia, gyromagnetic ratios and the energies of $\mu = 0$, $2'$ vibrations calculated at the static minima are compared with the experimental data in figs. 13–17. These figures require further explanation which is given below.

The basic parameters of the phonon model (B and C) and the rotational model (Q_s and $\mathscr{I}$) are related to the experimental E_{2+}, the energy of the first 2^+ state and

B(E2, 0 → 2). One method of comparing theory and experiment would be to plot E_{2+} and B(E2; 0 → 2) which would require the extraction of these quantities from the microscopically calculated B and C or Q_s and $\mathscr{I}$. However, it has been traditional to plot Q_s and $\mathscr{I}$ of the deformed nuclei (which form the bulk of those under con-

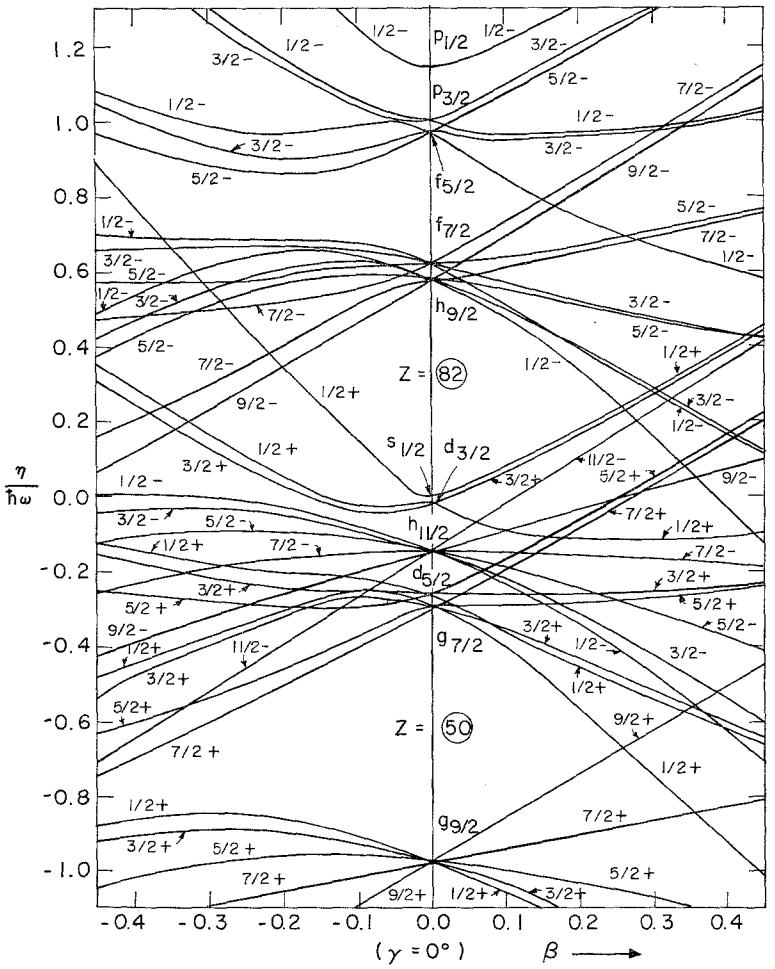

Fig. 11. Single-proton levels versus β. The plot is very similar to a Nilsson-diagram [36]) except that (i) the usual condition of volume conservation has not been used, and (ii) over and above the usual energy scale factor of $\hbar\omega = 41.2\ A^{-\frac{1}{3}}$ MeV, we have used a correction factor which takes into account the different number of protons and neutrons [both of these points have been discussed in ref. [13])]. The levels shown here correspond to $^{140}_{56}$Ba, $^{150}_{60}$Nd, $^{160}_{64}$Gd, $^{170}_{68}$Er, $^{180}_{72}$Hf, $^{190}_{76}$Os and $^{200}_{80}$Hg (nuclei with $Z/A = 0.4$). Energy levels for the other nuclei can be obtained by changing the β-scale by a factor of $(\frac{5}{2}ZA^{-1})^{\frac{1}{2}}$. Our choice of spherical ($\beta = 0$) levels has been discussed in sect. 1, and the numbers are given in table 1.

sideration). This procedure requires the extraction of these quantities from the experimental E_2 and B(E2; 0 → 2). One advantage of the traditional method is that

by looking at a plot of Q_s one can tell whether a nucleus is prolate ($Q_s > 0$) or oblate ($Q_s < 0$). This information cannot be obtained from a plot of $B(E2; 0 \rightarrow 2)$ which is proportional to Q_s^2. The apparent drawback of this method is that since the β_s and

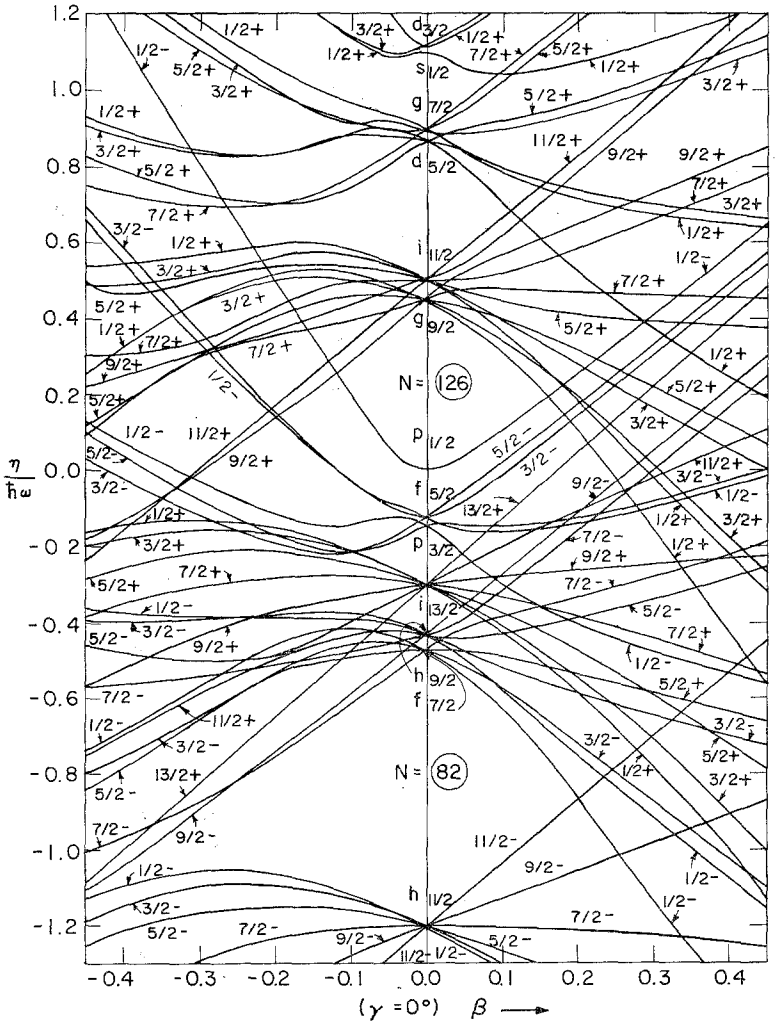

Fig. 12. Single-neutron levels versus β. The scaling factor (see the caption for fig. 11) for the β-axis is $(\frac{5}{3}NA^{-1})^{\frac{1}{2}}$.

the corresponding Q_s and $\mathscr{I}$ of a spherical nucleus vanish by definition, such plots would not yield any useful information about the spherical nuclei.

We combine the good features of the two methods of plotting in the following way. We plot Q_s and $\mathscr{I}$ for all nuclei of the region. Values for the deformed nuclei are obtained in the usual way. Those for the spherical nuclei are extracted from E_2

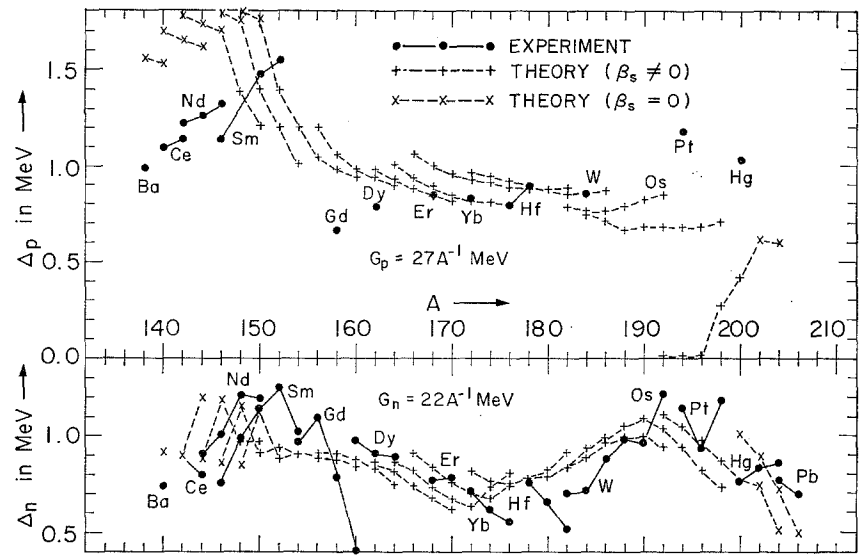

Fig. 13. Comparison with the experimental odd-even mass differences. Explanation for this figure is given in subsect. 2.2. Since Δ_τ(static) = 0 for a closed shell, such values have not been plotted. The experimental odd-even mass difference is then attributed to the gap in the single-particle levels. The calculated proton energy gap vanishes for $^{192-196}$Hg because the two single-particle levels near the Fermi surface at $\beta_s \approx -0.13$ (see table 2 and fig. 11) are separated by about 1.5 MeV which is an appreciable gap for a nucleus only two protons away from the magic number $Z = 82$. Shape fluctuations would cause mixing with the spherical solution for which $\Delta_p \approx 0.6$ MeV.

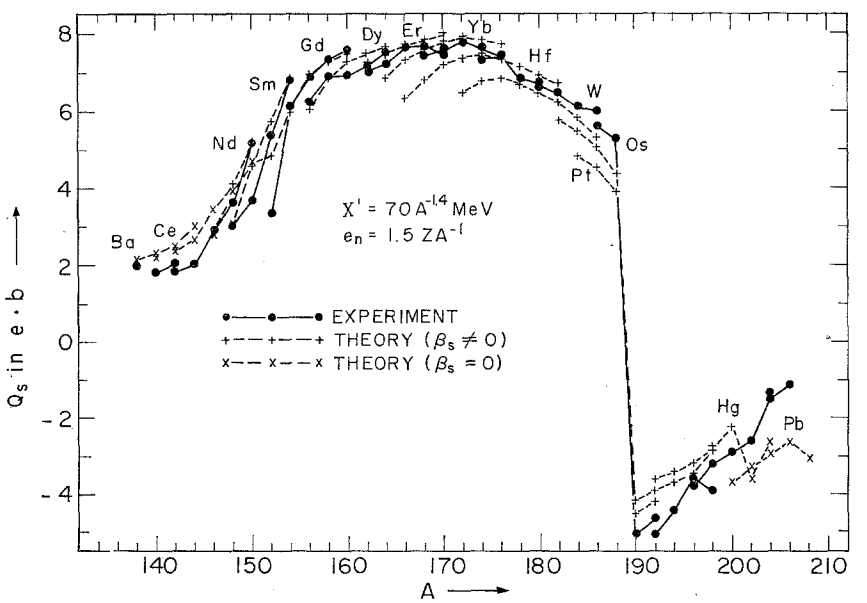

Fig. 14. Comparison with the experimental intrinsic quadrupole moments. A negative sign is used for both the theoretical and experimental values whenever the function $\mathscr{V}$ is lower on the oblate side than on the prolate side, even though its minimum may be at $\beta = 0$. Detailed discussion is given in subsect. 2.2.

and $B(E2, 0 \rightarrow 2)$ by combining the relations of the phonon and rotational models. Our somewhat unconventional procedure is in the spirit of the bold step taken by

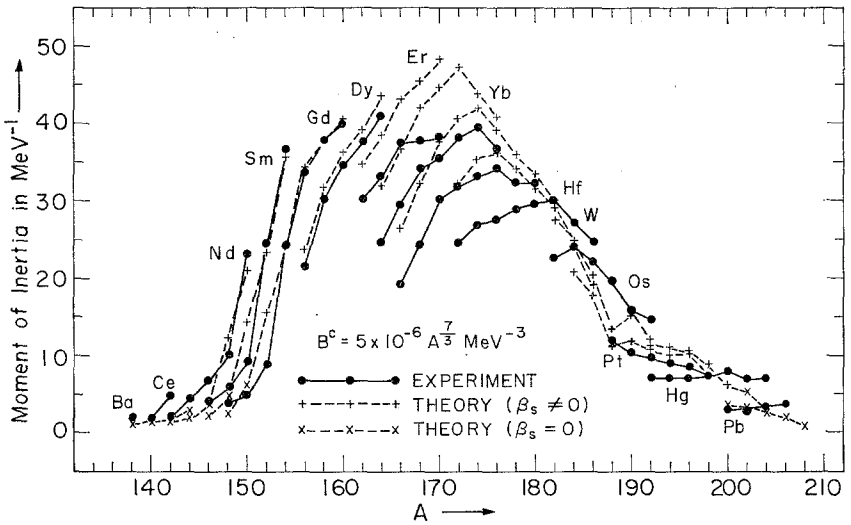

Fig. 15. Comparison with the experimental moments of inertia. Discussion is given in subsect. 2.2.

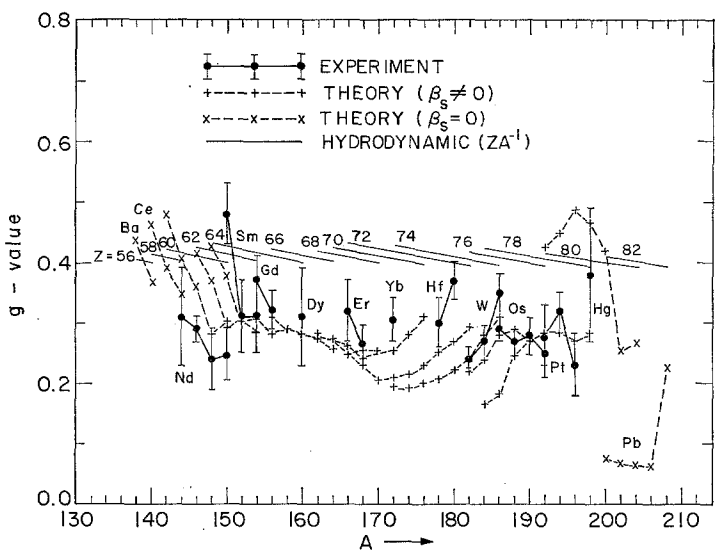

Fig. 16. Comparison with the experimental gyromagnetic ratios. Discussion is given in subsect. 2.2.

Stelson and Grodzins [1]) who tabulate $B(E2, 0 \rightarrow 2)$ and $\beta \approx [B(E2, 0 \rightarrow 2)]^{\frac{1}{2}}$ for all nuclei – including the spherical ones for which β is understood to be the rms value of the nuclear deformation.

The experimental quantities plotted in figs. 13–17 have been obtained by using the following relations. The odd-even mass differences (fig. 13) are obtained by using the Nilsson-Prior relations [20])

$$\Delta_p = \tfrac{1}{4}[3\{E(Z, N)-E(Z-1, N)\}+E(Z-2, N)-E(Z+1, N)], \tag{18}$$

$$\Delta_n = \tfrac{1}{4}[3\{E(Z, N)-E(Z, N-1)\}+E(Z, N-2)-E(Z, N+1)]. \tag{19}$$

The binding energies $E(Z, N)$ are taken from the mass table [25]). The table [1]) of

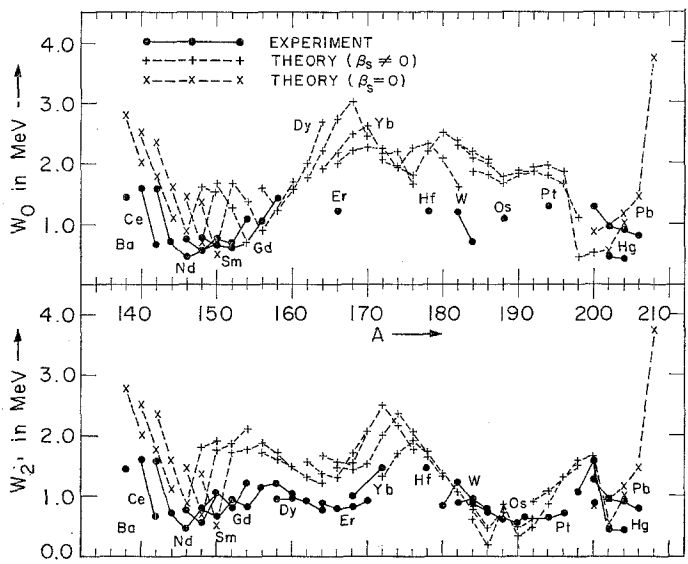

Fig. 17. Comparison with the experimental energies of $\mu = 0$ and 2′ vibrations. When the calculation gives $\beta_s = 0$, the energy $W_0 = W_{2'}$ = energy of a vibrational-phonon which is compared with the experimental energy of the first 2^+ state. When the calculation gives $\beta_s \neq 0$, the energies W_0 and $W_{2'}$ are compared with the experimental energies of the $0'^+$ and $2'^+$ states, respectively. These states represent the heads of the β- and γ-vibrational bands, respectively, when the deformed shape is axially symmetric. Compared to the experimental energies, the calculated values are in general too large by as much as a factor of 3. Part of the discrepancy may be attributed to the dynamic and anharmonic effects which can reduce the static values of β- and γ-vibrational energies by as much as a factor of 2 (see table 3). The remaining discrepancy is probably due to the breakdown of the adiabatic approximation since the two-quasi-particle states lie at about the same energies as the calculated values of W_μ. Better agreement with experiment has been obtained by Bès *et al.* [37]) and Pyatov *et al.* [38]).

B(E2, $0 \rightarrow 2$) is used to obtain the intrinsic quadrupole moment (fig. 14)

$$Q_s = [(\tfrac{16}{5}\pi)B(\mathrm{E2}, 0 \rightarrow 2)]^{\frac{1}{2}}. \tag{20}$$

A minus sign is used when it is required by the theoretical calculation. The experimental energy of the first 2^+ state [1,26,27]) is used to extract the moment of inertia

(fig. 15)

$$\mathscr{I} = 3E_{2^+}^{-1}. \tag{21}$$

The experimental value of the magnetic moment of the first 2^+ state [28,29]) is used to obtain the gyromagnetic ratio (fig. 16)

$$g = \tfrac{1}{2}\mu_{2^+}. \tag{22}$$

When the theoretical calculation gives $\beta_s = 0$, in fig. 17 we use the experimental [1]) value

$$E_{2^+} = W_0 = W_{2'}. \tag{23}$$

Otherwise, the experimental energies of the $0'^+$ and $2'^+$ states [26,27,30-32]) are used to obtain

$$W_0 = E_{0'^+}, \qquad W_{2'} = E_{2'^+}. \tag{24}$$

The theoretical values collected in table 2 and plotted in figs. 13–17 are determined in the following way. Values of Δ_τ and W_μ are obtained from eqs. (3)–(6) and eqs. (13)–(16), respectively. Values of Q_s, $\mathscr{I}$ and g are calculated as follows.

(i) When the calculated static shape is axially symmetric, the intrinsic quadrupole moment Q_s is obtained from eq. (8). Values of $\mathscr{I}$ and g are obtained from eqs. (9) and (10) for $k = 1$ or 2 ($\mathscr{I}_1 = \mathscr{I}_2 = \mathscr{I}$, $\mathscr{I}_3 = 0$; $g_1 = g_2 = g$).

(ii) When the static shape is spherical, the average values of Q_s and $\mathscr{I}$ are obtained by combining eqs. (20) and (21) of the rotational model and the following equations of the phonon model:

$$B(\mathrm{E2}, 0 \to 2) = \tfrac{4}{3}\tfrac{5}{2}\pi^{-2}Z^2R_0^4(BC)^{-\frac{1}{2}}, \tag{25}$$

$$E_{2^+} = (C/B)^{\frac{1}{2}}. \tag{26}$$

(Values of $B = B_0 = B_{2'}$ and $C = C_0 = C_{2'}$ are from table 2, and the relation $R_0 = 1.2\,A^{\frac{1}{3}}$ fm is used.) In this way, we include the effects of dynamics through the phonon model, and indeed the agreement with experiment seems to be good (figs. 14 and 15). Unfortunately, there is no simple way of including the effect of shape fluctuations on Δ_τ (static), which is given in table 2 and plotted in fig. 13. Undoubtedly, the dynamics would tend to reduce the effective Δ_τ since there is often a sharp reduction in the density of single-particle levels when the nucleus is deformed. In any case, the pairing-plus-quadrupole model is not capable of yielding absolute binding energies of individual nuclei so that complete agreement between the experimental odd-even mass differences and theoretical energy gaps should not be expected. The main purpose of such a comparison is to estimate the pairing force constants.

Since both the numerator and the denominator of the right-hand side of eq. (10) vanish at $\beta = 0$, the theoretical values of the gyromagnetic ratio (fig. 16) in the spherical case are obtained by computing [20])

$$g = \mathscr{I}_p/\mathscr{I} = B_p/B \qquad (\beta_s = 0), \tag{27}$$

where $B = B_0 = B_{2'}$ is given by eq. (15), and B_p includes the core contribution $B_p^c = g^c B^c$.

(iii) When the calculated static shape is asymmetric, more general relations than those used in (i) are required. The energy of the first 2^+ state of a rigid, asymmetric rotator is given by [24])

$$E_{2^+} = \mathscr{I}_1^{-1} + \mathscr{I}_2^{-1} + \mathscr{I}_3^{-1} - [(\mathscr{I}_1^{-1} + \mathscr{I}_2^{-1} + \mathscr{I}_3^{-1})^2 - 3(\mathscr{I}_1^{-1}\mathscr{I}_2^{-1} + \mathscr{I}_2^{-1}\mathscr{I}_3^{-1} + \mathscr{I}_3^{-1}\mathscr{I}_1^{-1})]^{\frac{1}{2}}. \quad (28)$$

Eq. (28) is combined with eq. (21) to deduce an effective $\mathscr{I}$. Values of Q_s and g are deduced by calculating $B(E2; 0 \rightarrow 2)$ and μ_{2^+} in this model [by diagonalizing the 2×2 rotational matrix and using the general relations given in ref. [19])] and combining with eqs. (20) and (22).

The comparison in fig. 16 shows that the correct order of reduction of g from the hydrodynamic value (Z/A) is obtained. This reduction has been attributed [20]) to the pairing force †. We also note (i) that the spin contribution to the g-value – which had been neglected in the Nilsson-Prior calculation [20]) – is about $\pm 15\,\%$; (ii) that some of the predicted g-values exceed the hydrodynamic value. This phenomenon of $g > Z/A$ has recently been observed [33]) in a different region of the nuclear chart.

One of us (K.K.) is grateful to Professor Hugh McManus for the hospitality of Michigan State University where part of this work was performed, and to Professor H. Feshbach for the hospitality of the Laboratory of Nuclear Science, MIT. We thank L. Grodzins and D. Murnick for communications concerning the experimental gyromagnetic ratios, E. Rost and E. Sanderson for information on the single-particle levels, S. Jha and R. Sorensen for many fruitful discussions in the early stages of this work and the staff of the LNS Computer Facility for extensive use of their services.

† Our results for the $A = 192$-200 isotopes of Hg show that an increase in the pairing force or the energy gap does reduce the g-value. The g-value increases rapidly in going from $A = 192$ to 196 because Δ_n decreases (while Δ_p remains constant). For $A = 198$-200, there is a sharp reduction in g because even though Δ_n is still decreasing, there is a sudden increase in Δ_p (see fig. 13 or table 2). These g-values are, however, nor reliable since these isotopes of Hg are rather weakly deformed (table 2) and hence transitional.

References

1) P. H. Stelson and L. Grodzins, Nucl. Data **1** (1965) 21
2) A. Bohr, Mat. Fys. Medd. Dan. Vid. Selsk. **26**, No. 14 (1952)
3) A. Bohr and B. R. Mottelson, Mat. Fys. Medd. Dan. Vid. Selsk. **27**, No. 16 (1953)
4) K. Alder *et al.*, Revs. Mod. Phys. **28** (1956) 432
5) J. M. Blatt and V. F. Weisskopf, Theoretical nuclear physics (Wiley, New York, 1958)
6) B. R. Mottelson and S. G. Nilsson, Mat. Fys. Skr. Dan. Vid. Selsk. **1**, No. 8 (1959)
7) S. T. Belyaev, Mat. Fys. Medd. Dan. Vid. Selsk. **31**, No. 11 (1959)
8) D. R. Bès and Z. Szymański, Nuclear Physics **28** (1961) 42
9) K. Dietrich, H. J. Mang and J. Pradal, Z. Phys. **190** (1966) 357
10) T. D. Newton, Can. J. Phys. **38** (1960) 700

11) S. Das Gupta and M. A. Preston, Nuclear Physics **49** (1963) 401
12) M. Baranger and K. Kumar, Nuclear Physics **62** (1965) 113
13) M. Baranger and K. Kumar, Nuclear Physics **A110** (1968) 490
14) M. Baranger, in Cargèse Lectures in theoretical physics, ed. by M. Levy (Benjamin, New York, 1963);
M. Baranger and K. Kumar, to be published
15) K. Kumar, Bull. Am. Phys. Soc. **7** (1962) 19; Ph.D. thesis, Carnegie Institute of Technology (1963) unpublished
16) M. Baranger and K. Kumar, in Perspectives in modern physics, ed. by R. E. Marshak (Wiley-Interscience, New York, 1966)
17) S. A. Moszkowski, Phys. Rev. **99** (1955) 803;
R. H. Lemmer and V. F. Weisskopf, Nuclear Physics **25** (1961) 624
18) G. Ripka, in Advances in nuclear physics, Vol. 1 (Plenum Press, New York, 1968)
19) K. Kumar and M. Baranger, Phys. Rev. Lett. **17** (1966) 1146;
Nuclear Physics **A92** (1967) 608 and to be published
20) S. G. Nilsson and O. Prior, Mat. Fys. Medd. Dan. Vid. Selsk. **32**, No. 16 (1960)
21) L. S. Kisslinger and R. A. Sorensen, Revs. Mod. Phys. **35** (1963) 853
22) J. Blomqvist and S. Wahlborn, Ark. Fys. **16** (1960) 545
23) S. Das Gupta and M. R. Gunye, Can. J. Phys. **42** (1964) 762
24) A. S. Davydov and F. Filippov, Nuclear Physics **8** (1958) 237;
J. P. Davidson, Revs. Mod. Phys. **37** (1965) 105
25) L. A. König *et al.*, Nuclear Physics **31** (1962) 18
26) K. Way *et al.*, Nuclear Data Sheets (National Research Council, Washington, D.C.)
27) F. S. Stephens, N. L. Lark and R. M. Diamond, Phys. Rev. Lett. **12** (1964) 225;
Nuclear Physics **63** (1965) 82;
N. L. Lark and H. Morinaga, Nuclear Physics **63** (1965) 466
28) I. Lindgren, in Perturbed angular correlations, ed. by E. Karlsson *et al.* (North-Holland Publ. Co., Amsterdam, 1965)
29) L. Grodzins *et al.*, Phys. Rev. Lett. **15** (1965) 369 and private compilations
30) T. Yamazaki *et al.*, University of California Radiation Laboratory Report UCRL-16986 (July 1966)
31) H. W. Baer *et al.*, Nuclear Physics **86** (1966) 332
32) J. J. Simpson *et al.*, Nuclear Physics **A94** (1967) 177
33) L. Grodzins *et al.*, Phys. Rev. Lett. **17** (1966) 1099 and references cited there
34) W. D. Myers and W. J. Swiatecki, Nuclear Physics **81** (1966) 1
35) H. E. Duckworth *et al.*, in Congr. Int. de physique nucléaire, Vol. II ed. by P. Gugenberger (Centre National de la Recherche Scientifique, Paris, 1964) p. 557
36) S. G. Nilsson, Mat. Fys. Medd. Dan. Vid. Selsk. **29**, No. 16 (1955)
37) D. R. Bès, Nuclear Physics **49** (1963) 544;
D. R. Bès *et al.*, Nuclear Physics **65** (1965) 1
38) N. I. Pyatov *et al.*, Joint Institute for Nuclear Research, Dubna, preprints (1966-67)